RSC Advances

PAPER

Cite this: *RSC Adv.*, 2020, **10**, 37735

An ICT-based fluorescence enhancement probe for detection of Sn^{2+} in cancer cells†

Xiangying Meng,[a] Lai You,[a] Siyuan Li,[a] Qi Sun,[b] Xiaogang Luo,[bc] Haifeng He,*[a] Jinglan Wang*[a] and Feng Zhao*[a]

Received 26th August 2020
Accepted 7th October 2020

DOI: 10.1039/d0ra07330j

rsc.li/rsc-advances

Development of a novel fluorescence enhancement probe for detection of Sn^{2+} in organisms, with high selectivity and sensitivity, is of great interest but remains a great challenge. Herein, an ICT-based fluorescence probe **TPPB** was rationally developed to act as an 'enhancement' luminescent and "naked-eye" indicator for Sn^{2+} detection. Importantly, spectroscopic studies indicated that **TPPB** was a fluorescence enhancement sensor for Sn^{2+} with rapid response, low detection limit (0.116 μM) and excellent binding constant (1.6×10^4 M^{-1}). The mechanism of **TPPB** response to Sn^{2+} was further proved by ^1H NMR titration, and enhancement calculations. Furthermore, **TPPB** is applied as a fluorescence probe for imaging in Hela cells, indicated that it can be potentially applied for Sn^{2+} sensing in biological fields.

Introduction

The study of the methods used to detect metal ions has attracted the interest of analysts and has been developed rapidly, due to the metal ions not being biodegradable.[1] Stannous chloride ($SnCl_2$) is a mild Lewis acid that is widely used as a reducing agent and catalyst in various synthetic organic operations and in the production of biodegradable polylactic acid.[2–4] In inorganic synthesis, $SnCl_2$, which acts as an effective reducing agent, could reduce metal salts, such as silver and gold salts to their metals, Cu^{2+} to Cu^{+}, and Fe^{3+} to Fe^{2+}.[5] Particularly, Sn^{2+} species have been used in articles of daily use, such as tin-plating of steel to make tin cans,[6] added to some canned and bottled foods,[7] and mouth wash.[8] In additional, tin is an essential trace micronutrient for living organisms.[9,10] For example, a deficiency of tin can enlarge the risks correlated with growth factors and cancer prevention, while an excess concentration of tin has a negative effect on the breathing, digestive, and nervous systems.[11] Therefore, it is significant to develop an accurate, simple, and efficient way to detect Sn^{2+}.[12]

Sn^{2+} ions have routinely been determined by flame atomic absorption spectrometry,[13] potentiometry,[14] voltammetry,[15] and UV-vis spectrophotometry.[16] Compare with these analytical approaches, fluorescent sensors have been developed for the determination of various important chemical species, as they offer significant advantages of excellent sensitivity, simplicity, instantaneous response and low detection limit up to nanomolar scale by contrast with routine analysis.[17–19] Therefore, the study of fluorescence probe as the high selectivity and sensitivity detection of Sn^{2+} is urgently desirable. Hitherto many of fluorescence probes for the detection of Sn^{2+}, which sensing mechanisms are mainly based on chemical reaction, complexation reaction, quantum dots, and nanoparticles, have been established.[20–22] However, Sn^{2+}-selective sensors base on chemical reaction and complexation reaction have rarely been reported.[23] Fluorescence probes, which based on complexation reaction between the probe and analyte, have become more and more precise, sensitive and popular in research. While the fluorescence quenching probe is more common in research when metal ions are bound to fluorophore receptor system, but other interference factors could cause the quenching of the fluorescence so that its sensitivity and selectivity will be reduced and inferior to the fluorescence enhancement probe.[24,25] Therefore, the fluorescence enhancement probe is highly preferable than the fluorescence quenching probe for practical applications about detecting heavy metal ions like Sn^{2+}, due to the higher sensitivity, selectivity, and reliability. The fluorescence enhancement probe is also quenched in heavy metal ions detection *via* enhancement spin–orbit coupling energy or electron transfer. For overcoming this challenge, sensors structures are often designed to contain specific moieties,[26–36] such as triphenylamine.[37] Recently, we have reported a probe of 2-

[a]*Jiangxi Engineering Laboratory of Waterborne Coating, School of Chemistry and Chemical Engineering, Jiangxi Science and Technology Normal University, Nanchang 330013, People's Republic of China. E-mail: hehf0427@jxstnu.com.cn; jxncwjl@163.com; zhf19752003@163.com*

[b]*Key Laboratory for Green Chemical Process of Ministry of Education, School of Chemistry and Environmental Engineering, Wuhan Institute of Technology, Wuhan, 430205, PR China*

[c]*School of Materials Science and Engineering, Zhengzhou University, No. 100 Science Avenue, Zhengzhou City 450001, Henan Province, PR China*

† Electronic supplementary information (ESI) available. See DOI: 10.1039/d0ra07330j

imidazole-pyridine derivatives with emission at 446 nm by utilizing the nitrogen of imidazole and pyridine to form complex with metal ion, but it shown fluorescence quenched behavior after coordinating with metal ion (Fig. 1).[38] In this work, Schiff base structural unit was designed to replace the imidazole to form weak electron-withdrawing center. Furthermore, diethylamino and triphenylamine moiety are strong electron-donating groups and thus are suitable as donor in an intramolecular charge transfer (ICT) system. The ICT process of free probe is weak due to the weak electron-withdrawing center. However, there is a strong ICT process after the N of Schiff base and pyridine coordinating with Sn^{2+} due to the weak electron-withdrawing center changing to strong electron-withdrawing center. The drastic change in ICT efficiency should elicit a fluorescence enhancement response.

Based on the above considerations, herein, we report a new ICT-based sensor **TPPB** (Fig. 1). Characterizations including ^1H and ^{13}C NMR spectra, and MS spectrum are utilized to confirm the chemical structure of sensor **TPPB**. The probe **TPPB** shows a fluorescence enhancement response to Sn^{2+}. This enables the probe to perform the detection of Sn^{2+} with good sensitivity, and prominent selectivity. Furthermore, the probe was successfully imaged for Sn^{2+} in living cells with low cytotoxicity. It is a suitable research tool to study the role of Sn^{2+} in a biological environment.

Experimental section

Materials and methods

All reagents for synthesis were analytically pure. All the solvents for spectroscopic measurement were chromatographically pure. ^1H NMR spectra were recorded at 400 MHz, in $CDCl_3$ solution on a Bruker AV400 MHz spectrometer and chemical shifts were recorded in parts per million (ppm) with TMS as the internal reference. Mass spectra (MS) were obtained on a QTRAP LC/MS/MS system (API2000; Applied Biosystems, Foster City, CA, USA), and signals were given in *m*/*z*. Fluorescence spectra were determined with a Hitachi F-4600 fluorescence spectrophotometer. Photoluminescence (PL) quantum yields were determined using a Hamamatsu system for absolute PL quantum yield measurements (type C11347).

Synthesis of compound TPPB

The synthetic method of compound **TPPB** was shown in Scheme 1. Compound 5-(4-(diphenylamino)phenyl)picolinaldehyde (**M-1**) was prepared according to the literature method.[39] Ethanol (10 mL), *N*,*N*-diethylbenzene-1,4-diamine (0.173 g, 1.05 mmoL) were stirred at room temperature, then, **M-1** (0.35 g, 1.00 mmoL) was added to the mixed solution under reflux for 2 h. After that the mixed solution was poured into 100 mL ice water, extracted with dichloromethane (3 × 30 mL), and evaporated under reduced pressure to remove the organic solvent. The product was isolated using silica gel column chromatography with petroleum ether/ethyl acetate = 5 as the solvent to yield faint yellow solid (0.39 g, 78.6% yield). ^1H NMR (400 MHz, $CDCl_3$) δ (ppm): 8.89 (s, 1H, Py-H), 8.70 (s, 1H, CH=N), 8.21 (d, J = 8.3 Hz, 1H, Py-H), 7.94 (d, J = 8.3 Hz, 1H, Py-H), 7.52 (d, J = 8.2 Hz, 2H, Ar-H), 7.38 (d, J = 8.5 Hz, 2H, Ar-H), 7.29 (t, J = 7.6 Hz, 4H, Ar-H), 7.16 (t, J = 7.0 Hz, 6H, Ar-H), 7.07 (t, J = 7.3 Hz, 2H, Ar-H), 6.72 (d, J = 8.6 Hz, 2H, Ar-H), 3.41 (q, J = 7.0 Hz, 4H, CH_2), 1.20 (t, J = 7.0 Hz, 6H, CH_3); ^{13}C NMR (100 MHz, $CDCl_3$) δ (ppm):154.57, 154.25, 148.70, 147.94, 147.82, 139.15, 136.82, 134.37, 131.18, 129.79, 128.15, 125.56, 125.23, 123.84, 123.64, 121.64, 112.44, 44.96, 13.08; EI-MS *m*/*z*: [M + 1] 497.3.

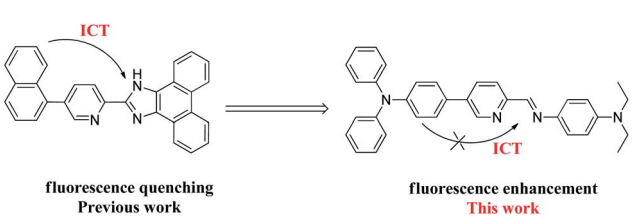

Fig. 1 Molecular structure of probe TPPB.

Results and discussion

Synthesis and characterization

The sensor **TPPB** was prepared according to Scheme 1. Initially the intermediates **M-1** was synthesized by the straightforward cross-coupling reaction under standard Suzuki coupling condition.[40] The Schiff base sensor **TPPB** was prepared in 78.6% yield as yellow solid from the condensation of 5-(4-(diphenylamino)phenyl)picolinaldehyde with *N*,*N*-diethylbenzene-1,4-diamine in ethyl alcohol under refluxing condition. ^1H NMR, ^{13}C NMR, and MS spectra were used to confirm the chemical structure of probe **TPPB**. All the protons and carbon atoms (Fig. S1–S3†) were unambiguous assigned.

Optical analysis of probe TPPB sensing Sn^{2+}

The selectivity of the **TPPB** probe for Sn^{2+} ion was researched by optical studies of the probe with various metal ions, and the sensitivity of the probe **TPPB** was also monitored by titration analysis. We firstly proceeded to examine the selectivity of the sensor **TPPB** to the various metal ions due to the selectivity is an important characteristic feature of an ion-selective sensor. We tested the selectivity of probe **TPPB** (20 μM) for Sn^{2+} (4.5 equiv.) with possible interferences including metal ion salts of K^+, Ag^+, Zn^{2+}, Pb^{2+}, Sr^{2+}, Mg^{2+}, Mn^{2+}, Hg^{2+}, Cd^{2+}, Ca^{2+}, Ba^{2+}, Cr^{2+}, Al^{3+}, Fe^{3+} (4.5 equiv.) in THF solution, respectively (Fig. 2A). Remarkably, only Sn^{2+} elicited a large fluorescence enhancement at 561 nm with excitation at 420 nm, due to the strong ICT process, which was resulted by the complexation of Sn^{2+} with N of pyridine and Schiff base, the electron-withdrawing ability of the recognition site was enhanced. By contrast, almost all the other interfering metal ions have no observable fluorescence response. Fig. 2B shown the color of the probe **TPPB** changed from very pale yellow to deep yellow with Sn^{2+} added under UV irradiation, while the color intensity of the probe **TPPB** did not change with other metal ions added, except that Al^{3+}, Cr^{2+} and Fe^{3+} brought about with slight enhancement. This may be due to the different electrical

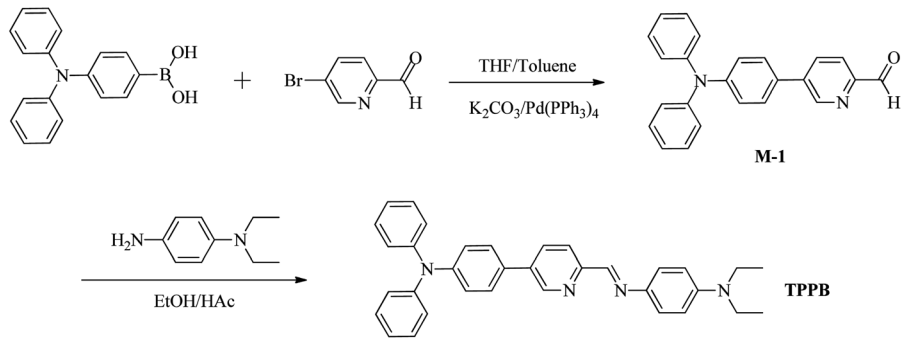

Scheme 1 The synthetic pathways of probe **TPPB**.

properties and inappropriate diameters of different metal ions. In Fig. 2C, the free **TPPB** can be seen as yellow solution. The color of the solution underwent change from yellow to colorless and transparent in the presence of Sn^{2+}, however other metal ions did not bring about any obvious change in the color of the solution, except that Zn^{2+}, Cd^{2+}, and Hg^{2+} brought about with yellow enhancement. So, **TPPB** can be used as visual indictor for Sn^{2+}. This technique is therefore superior to other analytical techniques because it has ability to detect Sn^{2+} by naked-eye.

Moreover, in order to explore the utility of **TPPB** as an ion-selective sensor, the competition experiments were carried out by adding other competitive metal ions to **TPPB** solution in presence of Sn^{2+} (Fig. 3). The black bar corresponds to the fluorescence probe **TPPB** with all of metal ions respectively, and red bar corresponds to the fluorescence probe **TPPB** with all of metal ions in presence of Sn^{2+} respectively. Interestingly, Sn^{2+} induced fluorescence responses were hardly influenced by these common coexistent metal ions. The evidence revealed that the probe **TPPB** shown a high selectivity and good stability toward to Sn^{2+} even in the presence of other relevant metal ions.

The sensitivity of the probe **TPPB** was monitored by titration analysis. The fluorescence titrations of **TPPB** with Sn^{2+} were

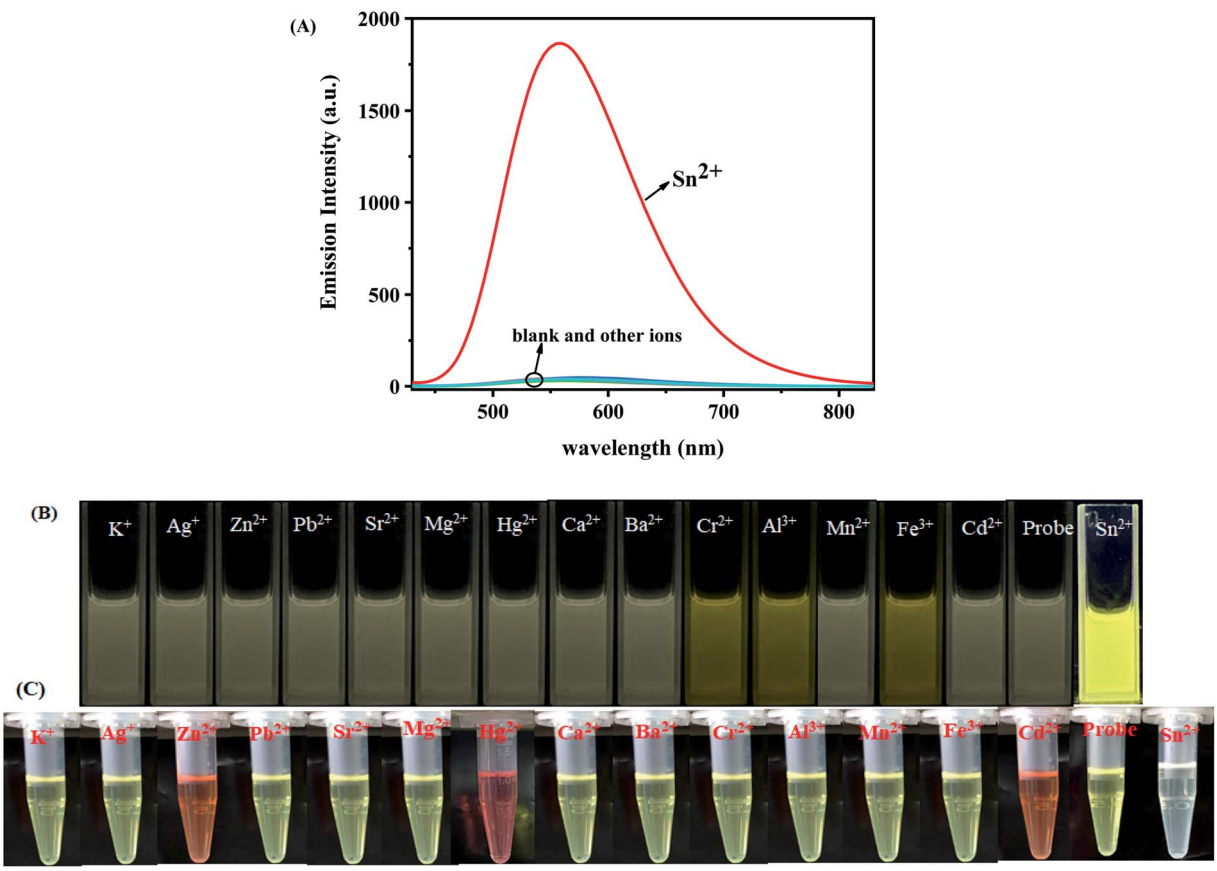

Fig. 2 (A) Fluorescence spectral of probe **TPPB** (20 μM) in the presence of Sn^{2+} (4.5 equiv.) and various of other metal ions (4.5 equiv.) in THF solution at room temperature, $\lambda_{ex} = 420$ nm; (B) the color changes of **TPPB** solution (20 μM) when a various metal ions (4.5 equiv.) were added under UV-light; (C) naked eyes color changes of the probe with different metal ions.

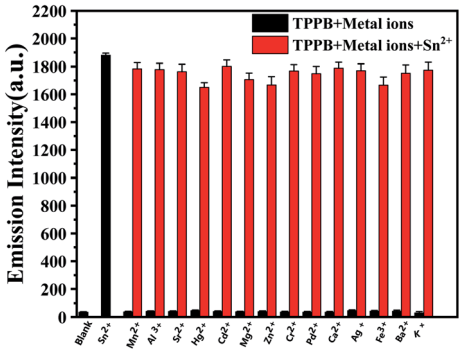

Fig. 3 Fluorescence response of TPPB with Sn^{2+} ion in coexistence of other metal ions at λ_{ex} = 420 nm, λ_{em} = 561 nm.

performed. As shown in Fig. 4A, probe **TPPB** exhibited extremely feeble fluorescence. However, with the addition of 0–4.5 equiv. of Sn^{2+}, the fluorescence intensity showed an excellent enhancement (up to 63-fold) at 561 nm. The fluorescence enhancement could be attributed to the strong ICT process.

The large fluorescence enhancement was corroborated by the observation that the fluorescence color of the sensor solution turned from very pale yellow to deep yellow (Fig. 4A, inset), which indicated that the probe **TPPB** showing an excellent fluorescence enhancement behavior for selective detection of Sn^{2+} ion. Subsequently, an evident increasing observed in the quantum yield (Φ) of [**TPPB** + Sn^{2+}] (68.21%) as compared to that of **TPPB** (1.43%) by using fluorescein (Φ_{ref} = 90%) as a standard fluorescence reference (the calculation formula see ESI S2.1†). It supports the fluorescence enhancement of **TPPB** observed in presence of Sn^{2+}, and suggesting a sensitive and selective detection of Sn^{2+} by **TPPB** compared to other metal ions. Importantly, the sensor shown a good linear relationship between the fluorescence intensity at 561 nm and the concentrations of Sn^{2+} from 1 to 6 μM (Fig. 4B), suggesting that sensor **TPPB** is potentially useful for quantitative determination of Sn^{2+} with a large dynamic range.

In order to confirm the binding stoichiometry between **TPPB** and Sn^{2+}, the Job's plots analysis was carried out. The plot of fluorescence intensity against the molecular fraction of [**TPPB**]/[Sn^{2+} + **TPPB**] was provided in Fig. S4A,† it showed the minimum at mole fraction of 0.5 indicating 1 : 1 stoichiometry between **TPPB** and Sn^{2+} in the complexes. Based on a 1 : 1 binding mode, apparent association constant (K_a) of the **TPPB**-Sn^{2+} interaction was calculated from the fluorescence titration spectra using the formula shown in calculation S2.3 (see ESI S2.3†) and K_a value was found to be 1.6 × 10^4 M^{-1}. What's more, a good linear relationship of the fluorescence intensity as a function of [Sn^{2+}] concentration from 0–4.5 equiv. (R = 0.99367) was obtained (Fig. S4B†). From the slope of the linear fit, the limit of detection (LOD) of the probe **TPPB** for Sn^{2+} ion was determined by using the formula shown in calculation S2.4 (see ESI S2.4†) and was found to be 0.116 μM (Fig. S4C†). Shortly, the probe **TPPB** could be a sensitive fluorescence probe for the quantitative detection of Sn^{2+} at micromole levels.

To further confirm the binding mechanism of Sn^{2+} with sensor **TPPB**, ^{1}H NMR titration experiments were performed in $CDCl_3$ and shown in Fig. 5. The changes in ^{1}H NMR signals of **TPPB** are more apparent with the appearance of the new peak around 10.10 and 8.99 ppm when the analyte concentration is 0.2 equiv., and subsequently, it becomes gradually intensified with further additions. Owing to the precipitation, we were unable to continue the experiment beyond 1.5 equiv. of Sn^{2+} ions. The new signals are assigned to the proton of H_a and H_c, which are located in the vicinity of Sn^{2+} binding site. The high field shift of 0.09 ppm for the arene proton (H_b) shows that the electron density has decreased around H_b after Sn^{2+} binding, due to the π-electron density shifted to the carbon, which link with N. On the other hand, the chemical shifts of H_d and H_e, shifted from 7.93(d) and 8.21(d) ppm to 8.01(s) ppm. These results indicated that N acted as electron donors for coordination to Sn^{2+}. The data further proved that the **TPPB** coordinating with Sn^{2+} with a stoichiometric ratio of 1 : 1.

DFT calculations

DFT studies further support the Sn^{2+}-assisted ICT process in **TPPB**. The optimized geometries of **TPPB** and **TPPB**-Sn^{2+} adduct, which were identified with the Job's plots analysis and ^{1}H NMR titration experiments, have been generated using B3LYP/6-311G(d, p) level (Lanl2dz for Sn) with Gaussian 09 software.[41] As shown in Fig. 6,

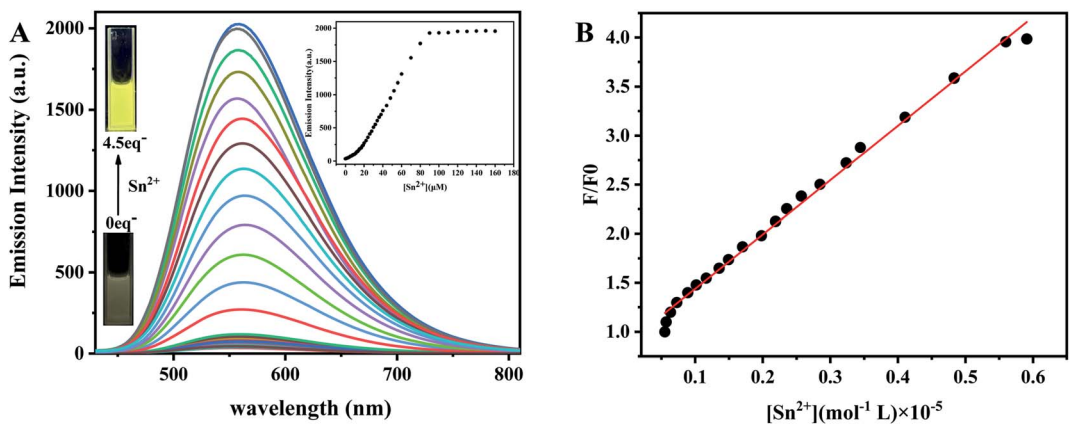

Fig. 4 (A) Fluorescence spectra of TPPB upon incremental addition of Sn^{2+} (0–4.5 equiv.). Insert: the fluorescence intensity of TPPB in the presence of increasing Sn^{2+} concentration; (B) the linearity between F/F_0 and Sn^{2+} concentration.

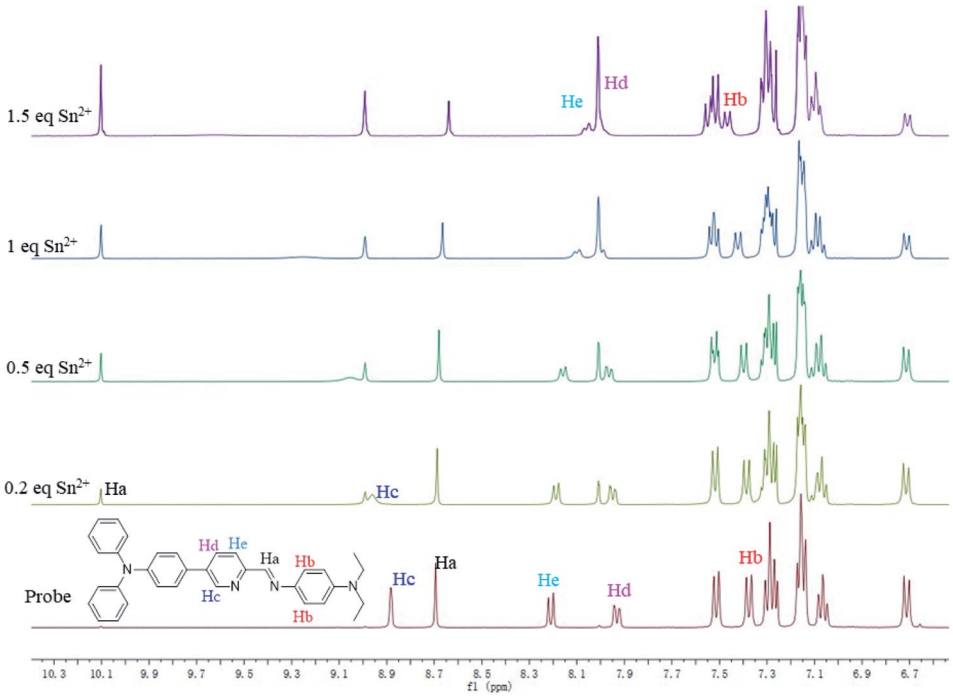

Fig. 5 ^{1}H NMR titration spectra of **TPPB** with Sn^{2+} ions in $CDCl_3$.

the N1 and N2 were found to be arranged in an almost in-plane orientation in **TPPB** and **TPPB**-Sn^{2+} adduct, with a dihedral angle of −179.3° and 1.9°, respectively. The planar conformation provides efficient π-conjugation. After optimizing structure of **TPPB**, the N1 and N2 were *trans*-configuration, while they convert to *cis*-configuration in **TPPB**-Sn. The above phenomenon means that the ground-state geometry undergoes a significant twist upon the addition of Sn^{2+}.

Examination of the frontier molecular orbitals given in Fig. 7 suggests that the electron density in the HOMO and LUMO for **TPPB** is entirely localized on the pyridine, Schiff base and one benzene ring of triphenylamine moiety. The above phenomenon clearly demonstrates an obstruction of the ICT process in **TPPB**, resulting in a weak fluorescence emission. While after Sn^{2+} ion binding with **TPPB**, the electron density localized on the Schiff base and triphenylamine moiety in the HOMO then shifted to Sn^{2+} binding site during transition to LUMO, which indicates an ICT from the Schiff base and triphenylamine moiety to the Sn^{2+} binding site, resulting in a strong fluorescence emission. Moreover, the calculated energy difference between HOMO and LUMO (0.53 eV) of **TPPB** –Sn^{2+} is lower than that of the free **TPPB** (the HOMO to LUMO energy gap is 3.18 eV). Hence, the ICT process of **TPPB**-Sn is also energetically favorable.

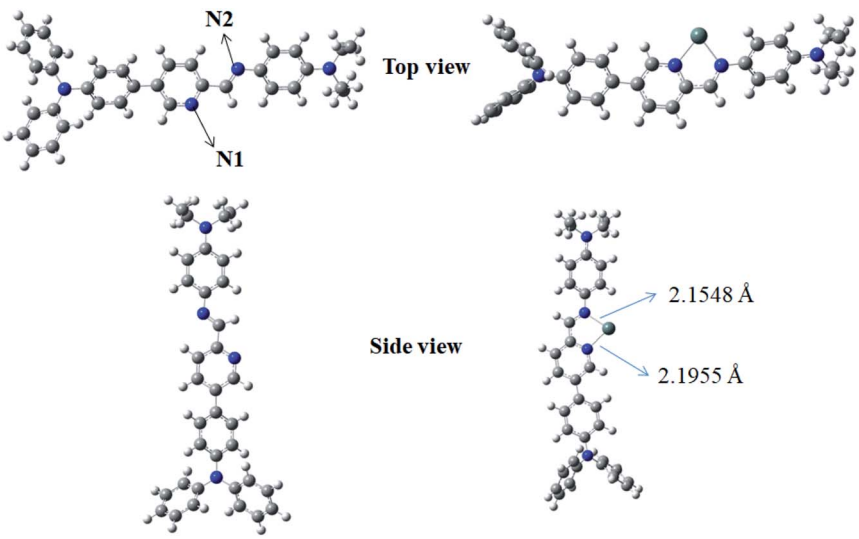

Fig. 6 The optimized geometric structures based on B3LYP for **TPPB** and **TPPB**-Sn^{2+}. Here, both top views and side views are shown.

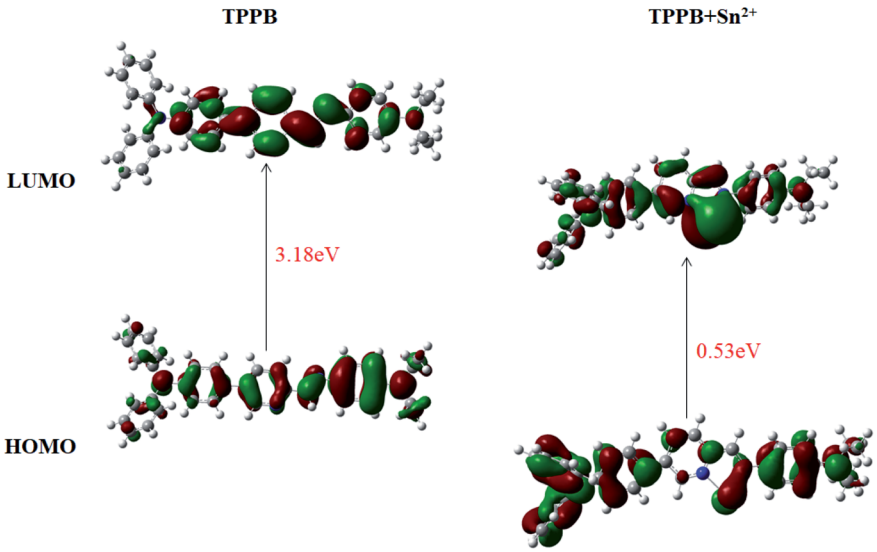

Fig. 7 HOMO–LUMO energy diagrams of **TPPB** with Sn^{2+} ions.

Imaging of cancer cell

In order to demonstrate the potential application of **TPPB** for the detection of Sn^{2+} in biological media, fluorescence microscopy studies were carried out by using Hela cells. The cytotoxicity of **TPPB** against Hela cells and normal cells was measured on MTT assay. The appropriate result was achieved based on Hela cells and normal cells, which showed high livability with more than 80% survival after 24 h (Fig. S5†). It means probe **TPPB** shows low cytotoxicity against cells.

Furthermore, **TPPB** as the fluorescence probe imaged in Hela cells for detection Sn^{2+} was studied. As shown in Fig. 8, incubation of Hela cells with 10 μM of the probe **TPPB** for 30 min gave very low dim fluorescence in the intracellular region (Fig. 8B). After treatment with 100 μM Sn^{2+} for 30 min, the fluorescence intensity obvious enhancement in Hela cells (Fig. 8E). These results inferred that the fluorescence realized enhancement due to the intracellular uptake of Sn^{2+} result in form of complex **TPPB**-Sn^{2+}. The above results providing direct

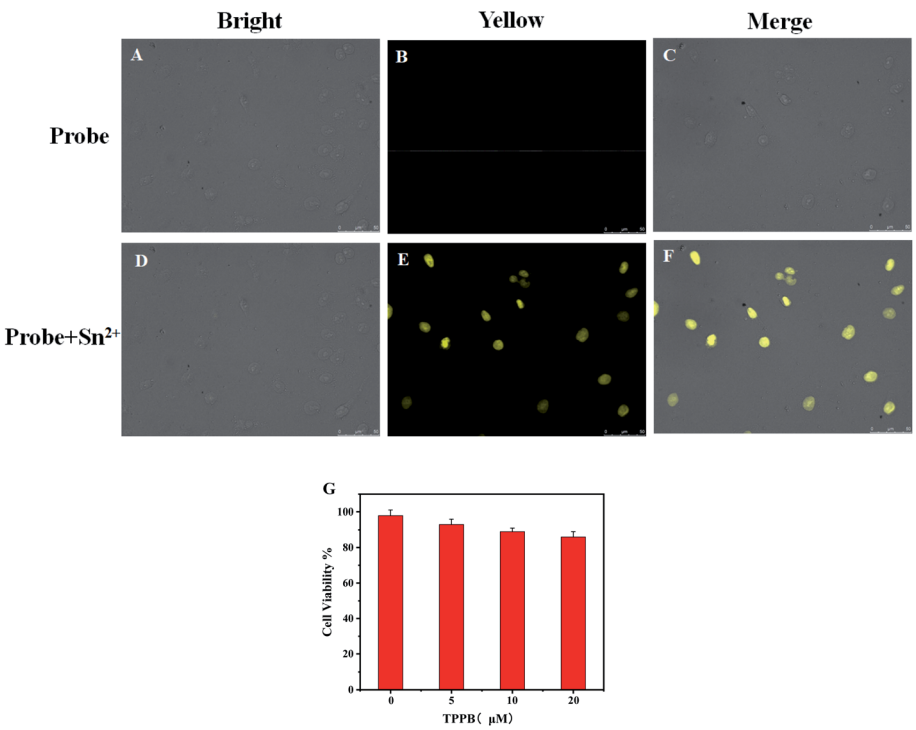

Fig. 8 Fluorescence imaging of Hela cells incubated with **TPPB** (20 μM) for 30 min (A–C), and then with Sn^{2+} (200 μM) for another 30 min (D–F), (Left) bright filed image, (Middle) yellow channel, (Right) merge image; (G) the cytotoxicity of **TPPB** against Hela cells incubated with different concentration of **TPPB** for 24 h.

evidence that the probe shows good biocompatibility with low cytotoxicity.

Conclusions

In conclusion, we have synthesized and characterized probe **TPPB** for detection Sn^{2+}. Interaction of Sn^{2+} with **TPPB** induces the fluorescence enhancement response with emission at 561 nm due to ICT process. Probe **TPPB**, which shows low detection limit of 0.116 μM and strong association constant of $1.6 \times 10^4\ M^{-1}$, is a highly sensitive and selective sensor toward Sn^{2+}, as demonstrated by selective, competitive and titration experiment. It could form complexes with Sn^{2+} with a stoichiometric ratio of 1 : 1. Importantly, the color of the probe **TPPB** changed from yellow to colorless and transparent with Sn^{2+} added under visible light, which meant that the probe can be used as visual indictor for Sn^{2+} by naked-eye. The possible recognition pattern was derived from DFT calculations, and ^1H NMR titration. Impressively, the probe **TPPB** with low toxicity has practical application in cell imaging, which indicated that the probe is suitable for tracking intracellular Sn^{2+}. In conclusion, **TPPB** can be used as a great promise candidate sensor for detection of Sn^{2+} in complex living samples.

Conflicts of interest

There are no conflicts to declare.

Acknowledgements

The authors are grateful for the financial support from the National Natural Science Foundation of China (21867011); Natural Science Foundation of Jiangxi Province (20192BAB213008); University (no. QD201907), the Outstanding Young and Middle-aged Scientific Innovation Team of Colleges and Universities of Hubei Province: "Biomass Chemical Technologies and Materials" (Grant No. T201908).

References

1 L. M. Zhu, J. Yang, Q. S. Wang and L. T. Zeng, *J. Lumin.*, 2014, **148**, 161–164.
2 O. M. Singh and L. R. Devi, *Mini-Rev. Org. Chem.*, 2013, **10**, 84–96.
3 R. G. Clevenger, B. Kumar, E. M. Menuey, G. H. Lee, D. Patterson and K. V. Kilway, *Chem.–Eur. J.*, 2018, **24**, 243–250.
4 Z. Q. Lei, Y. B. Bai and S. F. Wang, *Chin. Sci. Bull.*, 2005, **50**, 2390–2392.
5 X. Y. Yue, X. G. Zhang and F. L. Qing, *Org. Lett.*, 2009, **11**, 73–76.
6 L. J. Curtman and J. K. Marcus, *J. Am. Chem. Soc.*, 1914, **36**, 1093–1103.
7 F. M. El-Demerdash, M. I. Yousef and M. A. Zoheir, *Food Chem. Toxicol.*, 2005, **43**, 1743–1752.
8 A. Wieg and T. Attin, *J. Dent.*, 2014, **42**, 1210–1215.
9 H. Rüdel, *Ecotoxicol. Environ. Saf.*, 2003, **56**, 180–189.
10 Y. Arakawa and K. Tomiyama, *Nihon. Rinsho.*, 2016, **74**, 1199–1206.
11 N. Cardarelli, *Thymus*, 1990, **15**, 223–231.
12 A. K. Mahapatra, S. K. Manna, K. Maiti, R. Maji, C. D. Mukhopadhyay, D. Sarkar and T. K. Mondal, *RSC Adv.*, 2014, **4**, 36615–36622.
13 S. Ulusoy, H. İ. Ulusoy, M. Akçay and R. Gürkan, *Food Chem.*, 2012, **134**, 419–426.
14 I. A. Ismail and A. M. El-Kot, *Microchem. J.*, 1991, **44**, 49–53.
15 A. S. Dadda, A. C. Teixeira, P. K. Feltes, M. M. Campos, C. E. Leite and C. M. MoriguchiJeckel, *J. Braz. Chem. Soc.*, 2014, **25**, 1621–1629.
16 M. Arvand, A. M. Moghimi, A. Afshari and N. Mahmoodi, *Anal. Chim. Acta*, 2006, **579**, 102–108.
17 S. K. Kailasa, J. R. Koduru, M. L. Desai, T. J. Park, R. K. Singhal and H. Basu, *Trac-Trend. Anal. Chem.*, 2018, **105**, 106–120.
18 Z. Zhou, Y. Li, W. Su, B. Gu, H. Xu, C. Wu, P. Yin, H. Li and Y. Zhang, *Sens. Actuators, B*, 2019, **280**, 120–128.
19 H. Xu, B. Gu, Y. Li, Z. Huang, W. Su, X. Duan, P. Yin, H. Li and S. Yao, *Talanta*, 2018, **180**, 199–205.
20 J. Du, M. Zhao, W. Huang, Y. Deng and Y. He, *Anal. Bioanal. Chem.*, 2018, **410**, 4519–4526.
21 K. S. Patil, P. G. Mahajan and S. R. Patil, *Spectrochim. Acta, Part A*, 2017, **170**, 131–137.
22 F. Firdaus, A. Farhi, M. Faraz and M. Shakir, *J. Lumin.*, 2018, **199**, 475–482.
23 J. H. Baek, M. G. Choi, N. Y. Kim and S. K. Chang, *Sens. Actuators, B*, 2019, **284**, 562–567.
24 A. J. Moro, P. J. Cywinski, S. Körsten and G. J. Mohr, *Chem. Commun.*, 2010, **46**, 1085–1087.
25 Z. Xu, S. J. Han, C. Lee, J. Yoon and D. R. Spring, *Chem. Commun.*, 2010, **46**, 1679.
26 K. C. Song, M. H. Kim, H. J. Kim and S. K. Chang, *Tetrahedron Lett.*, 2007, **48**, 7464–7468.
27 J. Zhang, K. Zhang, X. Huang, W. Cai, C. Zhou, S. Liu, F. Huang and Y. Cao, *J. Mater. Chem.*, 2012, **22**, 12759–12766.
28 H. Wang and W. H. Chan, *Tetrahedron*, 2007, **63**, 8825–8830.
29 H. Mu, R. Gong, Q. Ma, Y. Sun and E. Fu, *Tetrahedron Lett.*, 2007, **48**, 5525–5529.
30 H. Yang, Z. G. Zhou, J. Xu, F. Y. Li, T. Yi and C. H. Huang, *Tetrahedron*, 2007, **63**, 6732–6736.
31 R. Dwivedi, D. P. Singh, S. Singh, A. K. Singh, B. S. Chauhan, S. Srikrishna and V. P. Singh, *Org. Biomol. Chem.*, 2019, **17**, 7497–7506.
32 L. N. Neupane, P. K. Mehta, J. U. Kwon, S. H. Park and K. H. Lee, *Org. Biomol. Chem.*, 2019, **17**, 3590–3598.
33 X. M. Meng, L. Liu, H. Y. Hu, M. Z. Zhu, M. X. Wang, J. Shi and Q. X. Guo, *Tetrahedron Lett.*, 2006, **47**, 7961–7964.
34 E. M. Nolan, M. E. Racine and S. J. Lippard, *Inorg. Chem.*, 2006, **45**, 2742–2749.
35 J. Wang and X. Qian, *Chem. Commun.*, 2006, 109–111.
36 Y. F. Cheng, D. T. Zhao, M. Zhang, Z. Q. Liu, Y. F. Zhou, T. M. Shu, F. Y. Li, T. Yi and C. H. Huang, *Tetrahedron Lett.*, 2006, **47**, 6413–6416.
37 Y. Y. Zhu, H. Y. Xia, L. F. Yao, D. P. Huang, J. Y. Song, H. F. He, L. Shen and F. Zhao, *RSC Adv.*, 2019, **9**, 7176–7180.

38 Y. Y. Zhu, Q. Sun, J. W. Shi, H. Y. Xia, J. L. Wang, H. Y. Chen, H. F. He, L. Shen, F. Zhao and J. Zhong, *J. Photochem. Photobiol., A*, 2020, **389**, 112244.
39 J. L. Wang, C. Y. Chai, S. X. Xu, F. Zhao, H. Y. Xia and Y. B. Wang, *Inorg. Chim. Acta*, 2019, **484**, 237.
40 N. Miyaura and A. Suzuki, *Chem. Rev.*, 1995, **95**, 2457.
41 M. J. Frisch, G. W. Trucks, H. B. Schlegel, G. E. Scuseria, M. A. Robb, J. R. Cheeseman, *et al.*, *Gaussian 09, revision A.01*, Gaussian, Inc., Wallingford, CT, 2009.

